JOURNAL OF GEOPHYSICAL RESEARCH, VOL. 101, NO. D14, PAGES 18,961–18,977, AUGUST 27, 1996

Microphysical and electrical evolution of a Florida thunderstorm 1. Observations

Jeffrey R French,[1] John H. Helsdon, Andrew G. Detwiler, and Paul L Smith
Institute of Atmospheric Sciences, South Dakota School of Mines and Technology, Rapid City

Abstract. This study deals with the microphysical and electrical evolution of a thunderstorm that occurred on August 9, 1991, during the Convection and Precipitation/Electrification (CaPE) Experiment in eastern Florida. During its approximately 1-hour lifetime, the storm was penetrated several times by the Institute of Atmospheric Sciences' T-28 aircraft at midlevels. It was also penetrated at low and middle-levels by a National Oceanographic and Atmospheric Administration (NOAA) P-3 and scanned by three radars, one of which had multiparameter capabilities, operated by the National Center for Atmospheric Research. Two stages of the storm's evolution are analyzed herein during which the storm grew to produce precipitation and lightning. The first stage, sampled during the first T-28 penetration at 5.25 km (−3°C) and the P-3 at 6.4 km (−10°C), was characterized by a 2- to 3-km wide updraft (maximum 14 m s^{-1}) with cloud liquid water contents up to 4 g m^{-3}, low concentrations of graupel at −10°C, and small to medium raindrops in concentrations of less than 200 m^{-3} at −3°C. A downdraft region also existed that was devoid of cloud liquid water, but contained graupel up to 2 mm. Radar data (Z_{DR}) are consistent with a coalescence-dominated precipitation generation mechanism followed by transport of drops in the updraft to heights with temperatures colder than −7°C, where freezing formed graupel that continued to grow by riming. Electrification during this stage remained weak. The second stage, sampled during the second and third T-28 penetrations and the second P-3 penetration, was characterized at midlevels by a narrower updraft and a more diffuse, broad downdraft separated by a 1- to 2-km wide transition zone. The updraft continued to show significant cloud liquid water (~2 g m^{-3}) with few precipitation particles, while the downdraft had very little cloud liquid with graupel in concentrations >1 ℓ^{-1}. The transition zone shared both updraft and downdraft characteristics. The increase in ice concentration was accompanied by a rapid increase in the electrification of the cloud with peak electric fields reaching −20 kV m^{-1} at T-28 altitude and the detection of lightning by ground-based sensors and pilot report. As time progressed, precipitation particle concentrations reached several per liter at midlevels in both updrafts and downdrafts. The observations are consistent with electrification through a precipitation-based mechanism involving the development of the ice phase.

1. Introduction

Questions dealing with the electrical nature of thunderclouds have been puzzling atmospheric scientists for centuries, yet most major advances in the field have come in only the last few decades. Despite these advances, many questions concerning charge structure, mechanisms for charge separation, and electrical effects on a thunderstorm's microphysical evolution remain largely unresolved.

It is unclear at this time exactly which mechanisms are primarily responsible for the electrification of thunderstorms. The convective hypothesis, first proposed by *Grenet* [1947] and later by *Vonnegut* [1953], attributes charge separation to the motion of charged cloud particles and small ions in the cloud updraft and in the downdraft at its edges. The inductive hypothesis, originally proposed by *Elster and Geitel* [1913] for raindrop/cloud droplet collisions, attributes charge transfer to the interaction of polarized hydrometeors in the presence of an ambient electric field and large-scale separation to gravitational sorting of the particles. This theory has been explored for virtually all types of hydrometeor collisions [e.g., *Latham and Mason*, 1962; *Aufdermaur and Johnson*, 1972; *Brooks and Saunders*, 1994]. The noninductive hypothesis has been developed through a set of laboratory experiments dating back to *Reynolds et al.* [1957]. It has been shown [e.g., *Reynolds et al.*, 1957; *Church*, 1966; *Takahashi*, 1978a; *Jayaratne et al.*, 1983; *Saunders et al.*, 1991] that charge will be transferred during rebounding collisions between graupel and smaller ice crystals in the presence of supercooled water. Large-scale charge separation then results from gravitational separation of the two different-sized hydrometeor species. A review of these theories along with their strengths and weaknesses in explaining observed electrical characteristics of thunderstorms is given by *Saunders* [1993, 1995].

Recently, several field investigations involving both remote and in situ measurements have been mounted to characterize the microphysical and electrical state of convective clouds in order to shed light on the question of charge separation. It is noteworthy that relatively few of these investigations have studied subtropical storms such as occur along the east coast of Florida. Studies of subtropical storms have involved radar analysis and ground-based electric field data to infer the interior electrical structure of the thunderstorms [e.g., *Jacobson and Krider*, 1976; *Krehbiel*,

[1]Now at Department of Atmospheric Sciences, University of Wyoming, Laramie.

Paper number 96JD01625.
0148-0227/96/96JD-01625$09.00

1981, 1986; *Krider*, 1989; *Lhermitte and Williams*, 1985; *Maier and Krider*, 1986; *Murphy et al.*, 1996]. The results have characterized the electrical structure of these storms (basically tri-polar) without characterizing the accompanying microphysics to aid in identifying the electrification processes.

Some studies have obtained in situ electrical and microphysical data from subtropical and tropical clouds. *Takahashi* [1978b] made balloon-borne, large-hydrometeor charge measurements in two maritime thunderstorms near Ponape, Micronesia. They exhibited different degrees of electrification correlated with lightning production. One storm, sampled prior to the initiation of lightning, had charges of both signs at levels from 0 to −60°C with a slight excess of positive charge at warmer temperatures and net negative charge at colder temperatures, reaching a maximum around the −40°C level The second storm was already producing lightning at the time it was sampled. This storm had a more distinct tri-polar structure with the net negative charge peaking at around −20°C. Takahashi inferred from these data that the upper positive charge was carried by ice crystals and the main negative charge was carried on graupel, which he found to be consistent with the noninductive riming mechanism.

Takahashi [1990] flew a balloon-borne particle imaging system, correlating low lightning frequency with low graupel concentrations below the −30°C level, and higher graupel concentrations, but lack of liquid water above the −30°C level. This lack of collocated graupel and liquid water would produce weak electrification via a noninductive riming process

Goodman et al. [1989] used a polarization-diversity radar in Alabama to examine clouds that were maritime in nature. They found that lightning occurred only after significant concentrations of ice were inferred to have formed based on multiparameter radar signatures. *Willis et al.* [1994] obtained observations from aircraft passes through a thunderstorm during CaPE. Electrified regions at the −7° to −10°C level within this storm contained graupel, relatively little cloud water, and either downdraft or a relative minimum within an updraft. The synthesis of these observations suggest that ice formation is a precursor to significant electrification in subtropical maritime storms.

In a study similar to the one described below, *Ramachandran et al.* [1996] examined two storms on the same day during CaPE using aircraft and multiparameter radar data. Both storms were in close proximity spatially and temporally and both exhibited a multicellular character. Both storms showed development of ice-phase precipitation through the freezing of supercooled raindrops and the growth of electric fields to tens of kV m^{-1} at the 6 km (−6°C) level subsequent to the initiation of ice. While the aircraft-measured electric fields were of comparable magnitude in both storms, only the more dynamically vigorous cells in the second storm produced lightning. In each of these cells, the time between the first freezing of rain and first lightning was between 10 and 12 min. They concluded that the observations were consistent with a charging mechanism involving collisions of cloud and precipitation particles in regions with modest amounts of cloud water above the 6-km level. Electrification to the stage of lightning was dependent upon the vigor of the updrafts and the maximum depth of the cloud

In this and a companion paper, we try to shed additional light on the relation between the microphysics and electrification of subtropical storms through the analysis of both observational data and an associated modeling study. In this paper, we deal specifically with the analysis of in situ and remotely sensed observational data from a thunderstorm that occurred on August 9, 1991, during CaPE The data were analyzed in detail in order to determine both the microphysical and electrical evolution of the storm. In section 2 we discuss the collection and analysis of the data from the August 9 storm. Section 3 covers the results of the data analysis. Section 4 summarizes the observations, and section 5 discusses how our results shed light on the questions raised earlier in comparison with other studies. A companion paper deals with the numerical simulations of this storm.

2. Data Set

Two main data sets were used in the analysis of this storm. Data collected by radars constitute the first set. The second set comprises in situ measurements made using a variety of probes on board instrumented aircraft The majority of the in situ data was collected by the South Dakota School of Mines and Technology T-28. Data collected by the National Oceanic and Atmospheric Administration's (NOAA) P-3 were also analyzed. Since our view of the evolution of this storm is highly dependent on the interpretation of these data, we feel it necessary to discuss the measurement devices used and how measurements made by each device were interpreted.

2.1. Radar Measurements

The storm on August 9 was continually scanned by three National Center for Atmospheric Research (NCAR) radars, CP-2, CP-3, and CP-4. Figure 1 shows the location of the storm in relation to the radar installations, Cape Canaveral, and the Melbourne Airport. Both the CP-3 and CP-4 Doppler radars operated in the C band, at wavelengths of 5.45 cm and 5.49 cm, respectively. During the August 9 storm, the antenna from CP-4 had elevation control problems Because of this, the radar data discussed in the following sections come from either the CP-3 or the CP-2 radar.

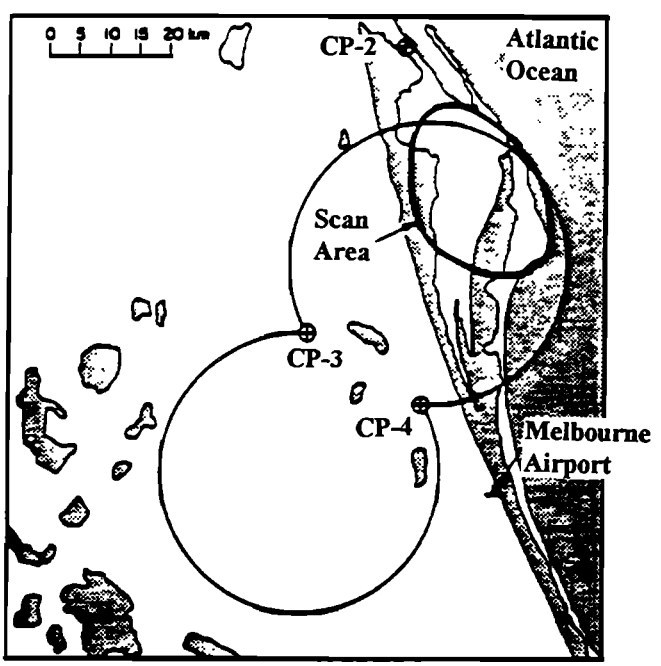

Figure 1. Location of August 9 CaPE storm in relation to radar sites and Melbourne Airport (base for T-28). The stippling indicates water. To the far right (east) is the Atlantic Ocean. The outer banks (Cape Canaveral) are separated from mainland Florida by the Banana and Indian Rivers. The scan area indicates the region in which the radars were scanning for this particular storm. Modified from *Foote* [1991].

The CP-2 was a dual-wavelength radar with multiparameter capabilities. It operated simultaneously in both the S band and the X band, corresponding to wavelengths of 10.68 cm and 3.20 cm, respectively. Both bands were able to provide reflectivity and Doppler data. In addition, the S band channel provided differential reflectivity, Z_{DR}, and the X band provided linear depolarization ratio (LDR).

Reflectivity data collected from CP-2 were compared to those collected from CP-3, and the two data sets compared well in both structure and value even though the CP-3 data used are raw reflectivity data, while the CP-2 data are gridded and smoothed. Both reflectivity fields were therefore used in the analysis of this storm. In addition, we analyzed the differential reflectivity field recorded by CP-2. Analysis of Z_{DR} played a vital role in determining the microphysical characteristics of this storm. Differential reflectivity is a measure of the difference in backscattered power from a wave both transmitted and received polarized horizontally as opposed to one polarized vertically. Mathematically, Z_{DR} is defined as

$$Z_{DR} = 10 \log \frac{Z_{HH}}{Z_{VV}} \tag{1}$$

where Z_{HH} represents the reflectivity factor due to horizontally polarized transmitted and received waves and Z_{VV} represents the reflectivity factor due to vertically polarized transmitted and received waves.

Our interpretations of Z_{DR} measurements were based on the conclusions reached by *Herzegh and Jameson* [1992]. Based on analyses of Alabama thunderstorms, they concluded that from Z_{DR} measurements one could clearly delineate regions of ice precipitation (Z_{DR}~0 dB) from regions of significant rain precipitation (Z_{DR}>2 dB). Further, it was noted that in convective systems, Z_{DR} can provide the information necessary to detect the presence of supercooled rain (liquid water drops above the 0°C isotherm). We refer the reader to *Bringi and Hendry* [1990] for further discussions on the topic of differential reflectivity and its usefulness in radar meteorology.

2.2. In Situ Measurements

Data collected from two instrumented aircraft were used in the analysis of this storm. The P-3 made two penetrations into the storm, one at 6.4 km mean sea level (MSL) (−10°C, ambient) about 2 min after first echo (~1825:00 UTC) and another at 4.1 km MSL (+3°C, ambient), 20 min after first echo (all altitudes referred to henceforth will be with respect to mean sea level, and all times will be with respect to universal time convention).

Data collected by the P-3 and used in this analysis include particle images from both the Particle Measuring Systems Inc. (PMS) two-dimensional imaging precipitation probe (2D-P) and cloud probe (2D-C). Operation of these probes is discussed further, below. Also used were vertical wind calculations based on inertial navigation data, true air speed, and angle of attack (described by *Willis et al.* [1994]). Liquid water concentrations were derived from measurements made by the King Liquid Water Probe [*King et al.*, 1985].

Last, we analyzed the two components of the ambient electric field derived from measurements made by four electric field meters on the aircraft. The two resolvable components of the electric field measured by the P-3 are the component that is vertical with respect to the Earth's surface and the component that is perpendicular to the plane's heading and horizontal with respect to the Earth's surface. *Willis et al.* [1994] describe the method used to calculate the electric field based on measurements from the field meters on board the P-3 Contrary to the sign convention used by Willis et al., in this discussion a positive vertical electric field (z component) refers to net negative charge above the aircraft, and a positive horizontal electric field (y component) refers to net negative charge to the right of the aircraft's flight direction. This sign convention corresponds to a right-handed coordinate system in which the positive x direction (a component not resolved in the electric field calculations) points out of the tail of the aircraft.

The T-28 made seven penetrations at 5.25 km (-3°C, ambient) throughout the storm's lifetime. The first penetration (1835:15) began at about 11 min after detection of first echo, and penetrations continued until the storm was well into its decaying stage. The T-28 made its last penetration (1920:00) about 55 min after first echo. Herein we discuss data collected during the first three T-28 penetrations, corresponding to times up to about 25 min after first echo (about 9 min after first lightning). The fourth penetration was made considerably south of the main reflectivity core. The remaining penetrations were made while the storm was in its decaying stage, after collapse of the "Z_{DR} column," indicating at this stage the lack of sufficient updraft to maintain supercooled raindrops aloft.

Measurements of cloud liquid water concentrations (CLWC) from the T-28 were made using a Johnson-Williams (JW) probe. The accuracy of this device is not as great as that of the King Probe. The JW responds mainly to liquid water in the form of droplets less than 30 to 50 μm in diameter. Recent intercomparisons between this JW and a King Probe flown simultaneously on the T-28 show that this JW tends to give readings ~1/2 those of the King Probe in warm-based clouds with broader cloud droplet spectra.

The vertical wind estimates (from the T-28) were based on changes in aircraft pressure altitude, pitch, and vertical acceleration, using a method described by *Kopp* [1985]. The noise level for these calculations is about 2-3 m s^{-1}. The vertical wind calculation may be biased by up to a few meters per second, positively or negatively, depending on the trim of the airplane. The baseline zero value should be taken as the value computed in straight-and-level flight just prior to cloud entry.

Data from two probes on the T-28 were used in analyzing particle sizes and types: a PMS 2D-P imaging probe and a foil impactor. In this analysis, determination of the phases (water or ice) of the hydrometeors was considered very important. Since the determination of water phase is somewhat subjective, we discuss how this was done.

The PMS 2D-OAP probes are imaging probes designed to record a two-dimensional image (or shadow) of each sampled particle. Each probe consists of a linear array of 32 photodiodes illuminated by a laser beam. The diode array is scanned repeatedly as particles pass through the beam, yielding a two-dimensional shadow image. The optics and optical paths differ between the 2D-P and 2D-C models, giving different effective resolutions. For the 2D-P probes on both the T-28 and P-3, the effective diode spacing is ~200 μm, while for the 2D-C probe on the P-3 the spacing is 50 μm.

Based on the shape of the particle image, one can often determine the phase of the hydrometeor. Water drops with diameters greater than ~600 μm tend to cant (elongation along an axis of ~45°) in the flow field around the probe [*Black and Hallet*,

1986]. Graupel particles, on the other hand, do not cant, and therefore tend to result in less regularly oriented images. Because of resolution limitations imposed by the 2D-P probe, it is difficult to determine phase for hydrometeors. For this reason we analyzed data collected by the foil impactor to help discriminate the phase of hydrometeors in regions penetrated by the T-28.

The foil impactor consists of a thin moving strip of aluminum (~7.5 cm wide and ~0.003 cm thick) that passes over a ridged drum behind an open window (with dimensions of 3.75 by 3.75 cm). As particles strike the foil, they leave ridged impressions. The ridges are spaced at 0.25 mm, which defines the resolution of the instrument; the minimum detectable size is approximately 0.5 mm. The foil is exposed and transported only when the pilot-activated "in-cloud" switch is on. At other times, the foil is not moving, and a metal shutter covers the foil at the window position. Each time the in-cloud switch is turned off, the shutter closes, and a punch mark is made in the foil. The foil moves at a constant speed (~3.4 cm s^{-1}) during a penetration, punch marks denote the boundaries between penetrations, and the times associated with these punch marks are recorded on the data system. Thus one can determine the location in the cloud that each particle struck the foil with an uncertainty of about 100 m (the nominal accuracy of the global positioning system receiver on the aircraft).

The method used to determine the phases of hydrometeors that left impressions on the foil is based on the shapes of the imprints. Water drops are assumed to leave circular impressions, while ice or ice-liquid combination particles are assumed to leave "splatter" marks. This is based on a report prepared by *Miller et al.* [1967]. Laboratory experiments discussed by *Knight et al.* [1977] produced similar results, but also demonstrated that water-drop and ice-sphere impressions were indistinguishable for particles less than ~3 mm in diameter. As the foil impressions were analyzed only for their character, and not for detailed concentration and size statistics, overlapping impressions in regions of high precipitation particle concentration did not hinder the analysis.

We carefully considered both sets of particle data (2D-P and foil impactor) before concluding what types of particles existed in a given region in cloud. Using these two sets of data, we could discriminate between water and ice regions in cloud for particles with diameters greater than a few mm with a reasonable degree of certainty.

In this work the primary emphasis is on precipitation particle measurements. Particle concentrations are estimated in two ways. A rough estimate of precipitation particle concentration can be obtained by dividing the PMS probe shadow/or count (the total number of particles counted per second) by the optical sampling volume swept out by the probe (~0.15 m^3 s^{-1}, for example, for the T-28 2D-P probe). This concentration includes all sizes of particles, from those just big enough to activate the probe while not leaving an image (~0.2 mm, for the 2D-P) to those so large that they could not be entirely contained within the sample volume. It also includes artifacts due to water streaming off probe tips, fogged optics, and other phenomena. The precipitation particle concentration can be estimated similarly from the foil impactor by dividing the number of valid impressions within an area of foil, by that foil area multiplied by the distance moved during the time of exposure (roughly 90 m per second of exposure).

A more rigorous estimate of precipitation particle concentration can be obtained using the image data recorded by the PMS probes along with timing information encoded into the image data. In regions with high particle concentrations, these probes are often limited by memory and data transfer rate constraints to obtaining images for only a portion of the total time in-cloud. However, the disadvantages of this intermittent sampling are mitigated by the ability to ignore for counting purposes those images that are obvious artifacts, and to compute an appropriate size-dependent sample volume for larger particles only partially imaged.

Data from the P-3, with both 2D-C and 2D-P probes, suggest that the latter seriously undercounts particles so small they trip the probe but are not imaged, i.e. smaller than ~0.4 mm. For larger sizes we believe our computed concentrations are representative of actual particle concentrations. One additional consideration in the concentrations computed from the T-28 2D-P probe in this study is that the images in the first halves of each 4 kilobyte buffer were often corrupted. This required concentrations to be estimated based on just half (the "good" half) of the total number of recorded images.

Determination of the electrical evolution of this storm relied heavily on measurements made by four electric field meters on the T-28. These four field meters are able to resolve two components of the ambient electric field, vertical and transverse to the direction of motion (the same as those resolved by the P-3). The field meters are model E-100, rotating-shutter type instruments described by *Winn* [1993].

The two field meters used to determine the horizontal (E_y) component of the electric field are located on the end of each wing tip. The two other meters (located on the bottom and top of the fuselage) are used to determine the vertical (E_z) component of the electric field. Details are presented by *Ramachandran et al.* [1996]. A brief summary is given here.

The four electric field meters in the four different positions respond differently to a unit-magnitude field component normal to their faces, due to differences in curvature and local surface features at each mounting location. The readings of the individual meters responding to the same field magnitude are scaled relative to each other using self-charging tests in negligible ambient fields and roll maneuvers in constant ambient fields with negligible self-charging. Each of the ambient field components is then computed by calculating the scaled differences from each pair of oppositely facing field meters and correcting for the roll and pitch (using simple trigonometry). Overall enhancement of the ambient electric field around the aircraft is accounted for by multiplying the measurements by an enhancement factor determined through in-flight intercomparisons with the New Mexico Institute of Mining and Technology's (NMIMT) Special Purpose Test Vehicle for Atmospheric Research (SPTVAR) as documented by *Giori and Nanevicz* [1992]. The electric field meters saturate in ambient fields of approximately ±200 kV m^{-1}.

When the aircraft is highly charged, as it often is during thunderstorm penetrations due to precipitation particle impacts, various locations on the airframe and propeller will discharge plumes of ions. These plumes distort the electric field sensed by the meters on the fuselage and wingtips and may introduce artifacts in estimates of ambient field components [e.g., *Jones et al.*, 1993]. Experience with the T-28 has shown that when the magnitude of the ambient field is greater than the field owing to charge on the aircraft (computed from scaled sums of readings from the wingtip pair of meters, using the same overall enhancement factor) signs of distortions like those described by *Jones et al.* [1993] are infrequent.

We feel that T-28 measurements are accurate within about a factor of 2, based on clear-air formation flight intercomparisons made during CaPE with the NCAR Sailplane and King Air, and through continuity of spatial structure in electric field estimates made during successive penetrations made by the T-28, P-3, and NCAR King Air in another storm on this same day (V.N. Bringi et al., Evolution of a Florida thunderstorm during the Convecton and Precipitation/Electrification Experiment: The case of 9 August 1991, submitted to *Monthly Weather Review*, 1995), and by the T-28 and P-3 in the storm described below. The effects of aircraft charging appear to be minimal in the electric field data discussed below, except possibly during the final P-3 penetration. During this penetration, aircraft charging was high; however, the variation across the cloud of the ambient electric field components still looks reasonable.

3. Analysis of Observational Data

3.1. Environmental Conditions

The storm on August 9 was located over the western edge of Cape Canaveral, above the field mill network operated by the Kennedy Space Center. The storm formed along a convergence boundary [*Bringi et al.*, 1993] Figure 2 shows a sounding from a radiosonde that was launched at 1810:00, 15 min before detection of first echo. The sonde was launched from a mobile Cross-Chain LORAN Atmospheric Sounding System (CLASS) facility approximately 3 km south of where the storm formed. It shows a conditionally unstable atmosphere (lifted index −3.5, *K* index 36.8) that is relatively moist throughout its depth. The shear is 16.1 m s^{-1} through the lowest 6 km, while the convective available potential energy (CAPE) for this sounding is 1872 J/kg. The CAPE value is characteristic of many subtropical thunderstorm environments both over land and over ocean [*Lucas et al.*, 1994]. The bulk Richardson number is 15.

3.2. Storm Evolution

When comparing data from this storm with data from other storms observed during CaPE, we came to the conclusion that this storm is somewhat atypical of other CaPE thunderstorms described in the literature. Although most of the measured parameters (i.e., CLWC, particle concentrations, etc.) were comparable to those measured in other storms, the overall structure seemed different. In particular, most of the other storms in CaPE developed a distinct multicellular structure with the individual cells relatively easy to distinguish on radar plots. This storm did not share that characteristic.

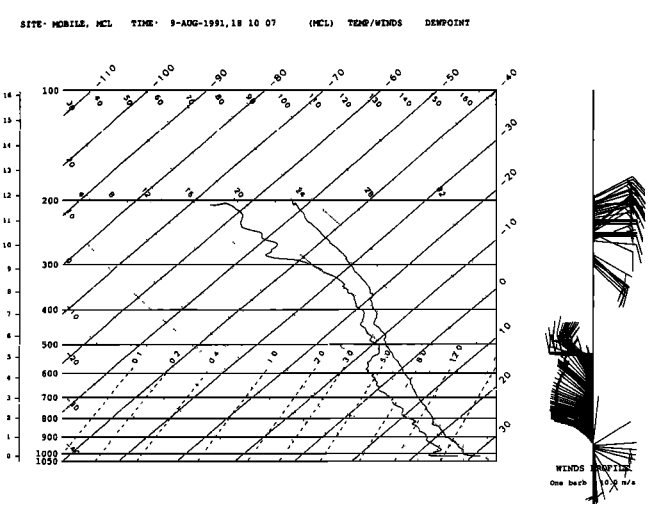

Figure 2. Plot of a sounding (temperature and dew point) launched by mobile CLASS at 1810:00 on August 9. The sonde was released approximately 3 km south of the storm's location.

Figure 3 presents a series of Constant Altitude Plan Position Indicators (CAPPIs) constructed from CP-3 data at four times during the observing period (1830, 1835, 1842, and 1849), from 5 min after first echo until the end of the third T-28 penetration. The different heights approximate the +3, −3, -10, and −20°C levels in the cloud, respectively. During the first three time periods, the cloud was essentially stationary and we believe characterized by a single updraft. This conjecture is supported by the presence of a single Z_{DR} column during this period (as discussed below). The presence of two distinct maxima in the reflectivity at 1842 in the 6 km and 5 km CAPPIs is likely to be precipitation cascading off the top of the nearly vertical updraft. There is an indication of the development of a second updraft region in the northeast quadrant by 1849, which is supported by the spreading of the storm in that direction in the 1849 column of Figure 3. While there is evidence for the development of a second cell within this cloud, it seems to occur after the original cell had evolved electrically to the point of producing lightning at or before 1842. So, we believe that what is described in the following discussion is the microphysical and electrical evolution of a single thunderstorm cell.

3.2.1. P-3 penetration 1. At about 1827:00, the P-3 penetrated this cloud at 6.4 km (−10°C, ambient) flying from the northwest to the southeast. The cloud at this time and altitude was only 2-3 km in diameter, with a peak reflectivity of 15 dBz near the penetration level. Aircraft-measured vertical winds at this level were all positive (maximum ~14 m s^{-1}). The King Probe indicated a peak CLWC value of 4 g m^{-3}. Table 1 indicates that the 2D-C and 2D-P probes encountered a few small precipitation-size particles, none larger than 1 mm. Electric fields (both horizontal and vertical) encountered by the P-3 were less than 2 kV m^{-1} and may have been influenced by a mature storm located a few kilometers to the southeast. These measured electric fields were smaller than the uncertainty of the measurements [*Willis et al.*, 1994].

3.2.2. T-28 penetration 1. The maximum reflectivity in the cloud reached 20 dBz by 1830:00, and 45 dBz by 1835:00. The T-28 began making its first penetration 8 min after the P-3, entering cloud at 1835:15. Flying from the southeast to the northwest, the aircraft penetrated at an altitude of 5.25 km (−3°C, ambient). Figure 4 shows a CAPPI of reflectivity at 5.25 km. These data were collected from CP-2 near and during the time of the first penetration; the CP-2 site is the origin for the coordinate system used. In the southeastern half of the cloud, the T-28 flew through an area of relatively high reflectivity (in excess of 40 dBz). In the northwestern half, the reflectivities were much lower, between 20 and 40 dBz.

The lower panel in Figure 5a shows a vertical cross section of CP-2 reflectivity along the flight path of the T-28. The ordinate is altitude above ground, and the abscissa is plotted in time units but can be thought of as a spatial variable. Since the T-28 was flying at approximately 90 m s^{-1} (although the true air speed varies between 80 and 105 m s^{-1}), each 10 s represents ~0.9 km of data. The two graphs above the reflectivity cross section show the 2D-P shadow/or count, which represents the number of times

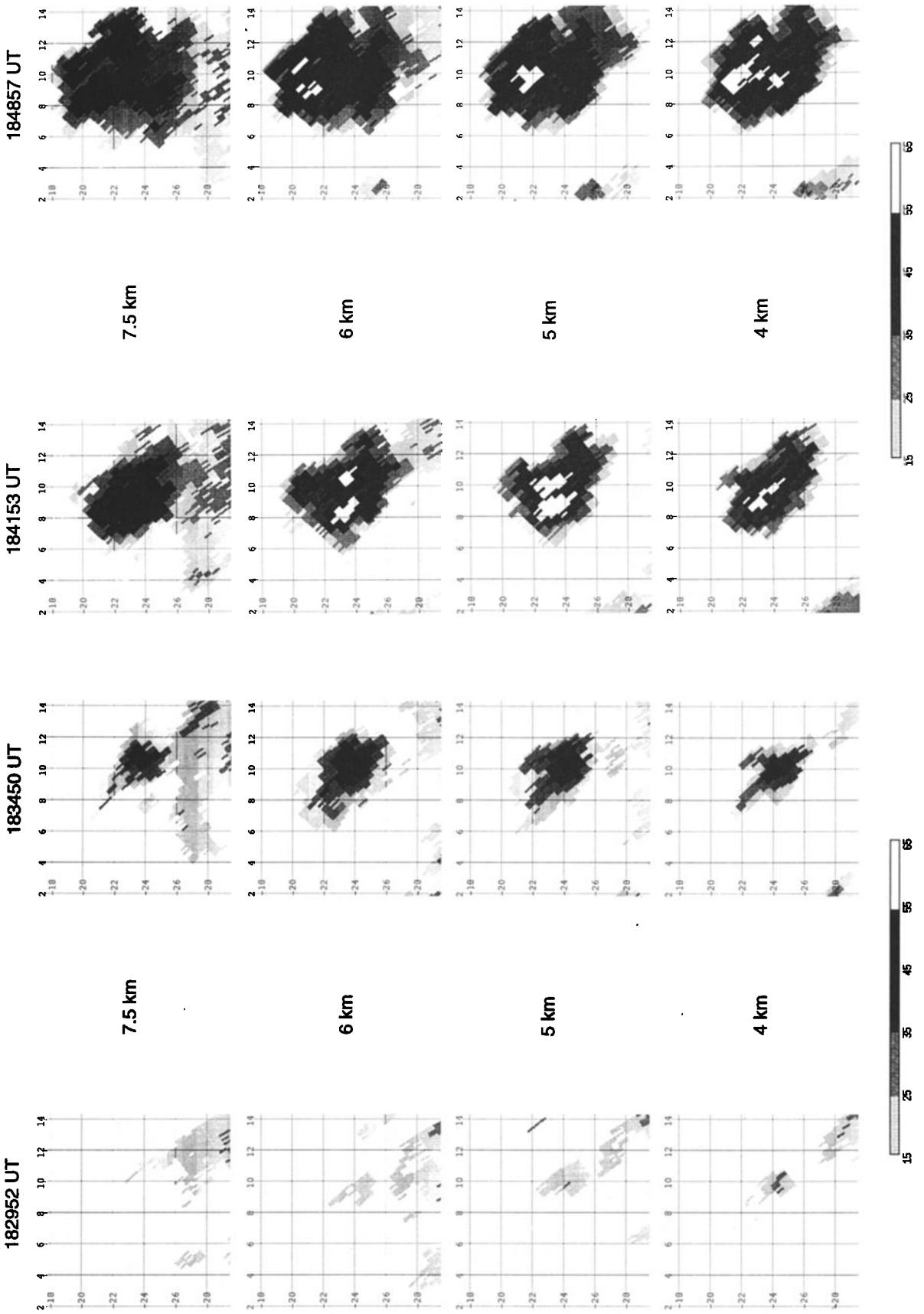

Figure 3. A series of CAPPIs at 4, 5, 6, and 7.5 km (+3, -3, -10, and -20°C) for 1830, 1835, 1842, and 1849 generated from CP-3 data. The Cartesian grid represents distance (in km) from CP-2. The gray scale at the bottom indicates reflectivity from 15 to 65 dBz in increments of 10 dB. The data are unsmoothed reflectivities, hence the blockiness of the plots.

Table 1. Microphysical Characteristics of the Different Cloud Regions Discussed in the Text

Begin	End	Alt, km	T, °C	Max CWC	VW	Total	≥400 mm	≥ 1mm	≥2mm	≥3 mm	Max D, mm	Phase
P-3	**Pen 1**	6.4	−10									
1826:57	1827:06			4	up	220	35				0.95	ice
T-28	**Pen 1**	5.2	−3									
1835:15	1835:21				dn	2400	370	16			1.6	ice
1835:27	1835:27				dn	2700	690	100	16		2.4	ice
1835:28	1835:40				dn	2600	790	260	80	37	7.5	ice
1835:40	1835:44				dn	2000	430	21	9	6	7.4	mixed
1835:50	1836:24			2	up	2900	160	32	6	3	3.4	liquid
T-28	**Pen 2**	5.2	−3									
1840:48	1840:51			2	up	1200	300	64	10	10	5.6	liquid
1840:51	1840:59			2	up	1300	200	29	12		2.6	liquid
1841:00	1841:09			1.5	tr	2900	420	74	19	9	6.6	mixed
1841:10	1841:20				tr	3800	680	72	10	6	6.8	mixed
1841:20	1841:48				dn	4800	1700	690	110	41	7.2	ice
P-3	**Pen 2**	4.1	3									
1845:10	1845:40				dn	850	530	190	35	5	7.2	ice
1845:40	1846:16			3	up	1100	460	110	15	5	9.5	mixed
T-28	**Pen 3**	5.2	−3									
1847:51	1847:54				dn	4800	280				0.8	ice
1847:55	1848.00				dn	4000	340	34			2.4	ice
1848:00	1848:18				dn	3800	1000	320	120	41	6.6	ice
1848:18	1848:30				tr	5900	1800	620	250	160	6.3	mixed
1848:30	1848:40			0.8	up	2100	730	350	200	130	7.6	mixed
1848:43	1849:00			0.3	dn/up	3400	1000	370	120	36	5.6	mixed

"Begin" and "end" columns delimit the time interval when the aircraft passed through the region, Alt is the average geopotential altitude, T is the average temperature, Max CWC is the maximum cloud water concentration encountered during the period, VW characterizes the region as updraft (up), downdraft (dn), or a transition (tr) between the two. Total is the total particle concentration of particles larger than 200 μm (estimated from 2D-P probe observations except for the first P-3 penetration, where the estimate is based on a 2D-C probe) while the succeeding columns denote the number larger than or equal to the indicated size In the final column, Phase notes the predominant phase of the hydrometeors encountered during the period.

per second the 2D-P probe was "tripped" (top), and the vertical electric field component (bottom) as computed from T-28 field meters. Figure 5b shows a corresponding cross section of differential reflectivity along the flight path of the T-28. The two graphs above this panel show the CLWC measured by the JW probe (top) and the vertical wind (bottom).

Referring to Figures 5a and 5b, it is apparent that as the T-28 flew through the southeastern half of the cloud (1835.15 to 1835:50) it encountered a downdraft with vertical velocities between −5 and −10 m s^{-1}. As mentioned earlier, the reflectivity values were highest in this portion of the cloud. Also, as one would expect, the 2D-P shadow/or counts, proportional to precipitation particle concentration, were relatively high in this portion. In the northwestern half of the cloud (1835:50 to 1836 30) the T-28 encountered moderate updrafts with vertical winds between 5 and 15 m s^{-1}. The reflectivities and shadow/or counts here were generally lower, except for one local peak in shadow/or counts near 1836:20, on the northwest edge of the strongest updraft, where the highest concentrations of the penetration were encountered. These concentrations are relatively low (~300 m^{-3}) compared to those that eventually develop in the storm.

In the downdraft portion (1835:15 to 1835:50), Z_{DR} values (at the level of the T-28) were low, less than 1 dB. This is indicative of an area made up mostly of ice particles or small water drops. In the updraft portion, where the reflectivity was rather weak, Z_{DR} values as great as 3.5 dB were measured at the level of the T-28. The "high Z_{DR} column" (1.5 dB contour) was found to extend up to a height of 7 km (−15°C, ambient). This is indicative of an area in which relatively low concentrations of larger liquid water drops are present. Also, CLWCs in the updraft were relatively high (maximum of ~1.7 g m^{-3} as measured by the JW probe), while the downdraft was virtually devoid of any cloud liquid water.

A sample of particle images detected by the 2D-P probe during the downdraft in the first penetration is shown in Figure 6a. Particle concentration statistics are given in Table 1. This downdraft region is far from being homogeneous in particle size, habit (shape), and concentration. In the southeasternmost portion of the downdraft (through 1835:21), the 2D-P probe detected a relatively low concentration (~10 m^{-3}) of graupel particles, all in the 1- to 2-mm size range. For the next 7 s (~630 m) the T-28 flew through a region of predominantly smaller particles (less than 1 mm in diameter) with a much greater concentration. From 1835:28 until 1835:40, the 2D-P probe detected a considerably broader size distribution with hydrometeors up to 7 mm in diameter. Both the 2D-P and the foil impactor data indicated that all of the particles in the downdraft up to this point were in the ice phase; this is consistent with the concurrent low values of Z_{DR}.

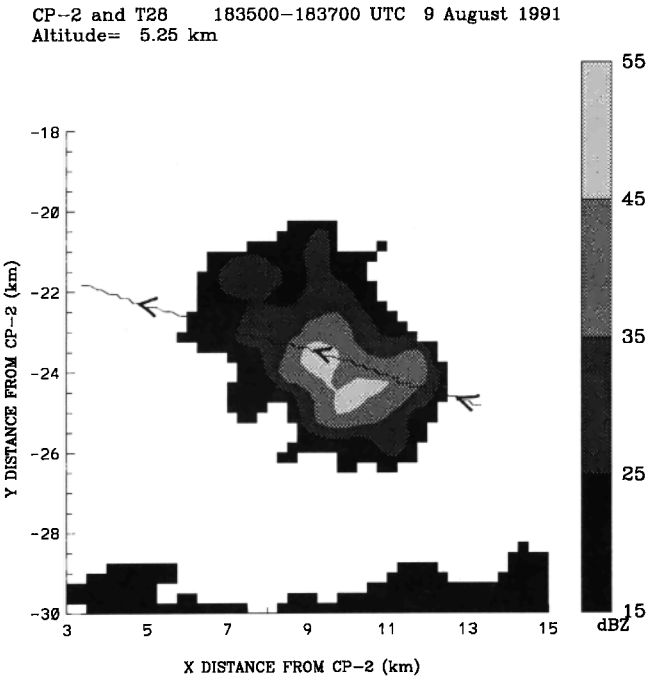

Figure 4. A CAPPI display at 5.25 km constructed from gridded and smoothed CP-2 data between 1835:00 and 1837:00 during the first T-28 penetration. The solid line indicates the flight path of the T-28 (SE to NW). The origin for this figure is the CP-2 radar site. Reflectivities are plotted from 15 to 55 dBz in increments of 10 dB as indicated by the scale on the right.

As the T-28 flew through the northwesternmost kilometer of the downdraft (1835:40 to 1835:50) Z_{DR} increased from 0 to about 1.5 dB. In this region, the 2D-P probe detected an average concentration of 9 m^{-3} of particles with diameters 2 mm or greater. Both the 2D-P and foil impactor data indicated that some of the particles were in the ice phase (graupel) and some were in the water phase (raindrops).

The T-28 entered the updraft at 1835:50. The entire 4-km width of the updraft (at 5.25 km) was characterized by high Z_{DR} (greater than 1.5 dB), relatively high CLWC, and low concentrations of precipitation-size particles. During the first 2 s that the aircraft was in the updraft (~180 m), the 2D-P probe detected a local concentration of more than 40 particles m^{-3} with diameters greater than 1 mm (Figure 6b). The 2D-P images and foil imprints indicate that all of these hydrometeors were water drops. Throughout the remainder of the updraft, neither the 2D-P probe nor the foil impactor detected any particles greater than 1.5 mm in diameter. During this 2.9 km of the updraft penetration, the 2D-P probe and foil impactor each would have sampled 4.6 m^3 of cloud. The reflectivity in this region must have been dominated by large drops in concentrations too low to be detected by the T-28 probes [cf. *Illingworth*, 1988]. Toward the middle of the updraft, a large number of very small (d < 0.4 mm) particles were detected. The phase (water or ice) of these drizzle-drop size hydrometeors could not be determined because of the resolution limit of the instruments; however, in an updraft at the penetration temperature of −3°C, one would expect them to be liquid. The 2D-P probe also imaged a large number of "streakers" (long, thin images caused by water flowing off the probe tips), which are indicative of relatively higher CLWCs.

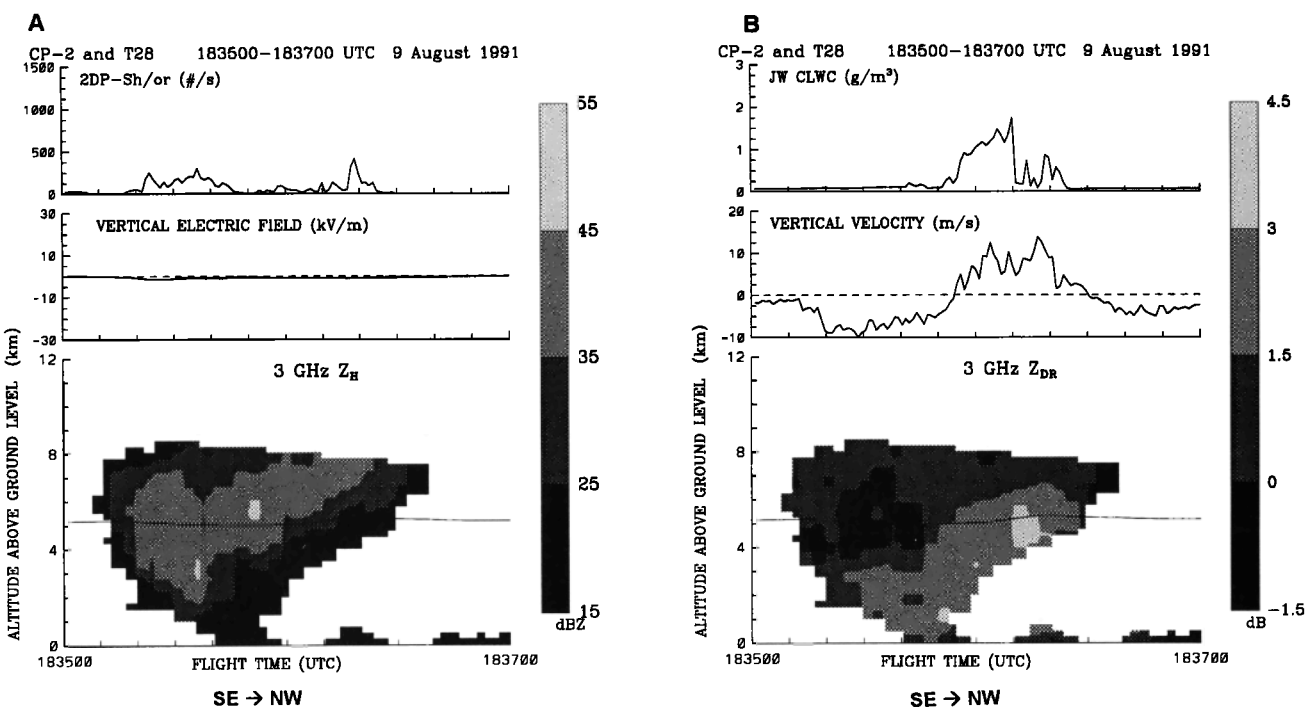

Figure 5. (a) The lower panel shows a reflectivity cross section along the flight track of the T-28 during its first penetration. The upper panels indicate the vertical electric field derived from the fuselage mills and the shadow/or count derived from the 2D-P probe. (b) The lower panel shows a Z_{DR} cross section along the T-28 flight path. The upper panels indicate the vertical wind calculated from T-28 measurements and the cloud liquid water concentration (CLWC) derived from the JW probe. Each tic on the abscissa indicates 10 s of flight time, or about 0.9 km of aircraft travel.

Figure 6. A sample of particle images recorded by the 2D-P probe from the (a) downdraft and (b) updraft during the first penetration. Vertical bars represent the 6.4-mm width of the probe aperture. Each line corresponds to one buffer (4 kbytes of data). The buffer headings show the buffer number, the start time of each buffer (format is 183533.35 = 1800 hours, 35 min, 33.35 s, for example) and the duration, or total elapsed time during which images were recorded, in decimal seconds. It takes a finite time for the data to be dumped to the data recording system; during this time, no data are recorded by the probe. Therefore this record represents a noncontinuous set of particle images. Only selected buffers are shown.

The existence of these streaker images in the PMS data supports the measurements of up to nearly 2 g m^{-3} of CLWC made by the JW probe. The T-28 exited the cloud at 1836:30.

The electric fields (both the vertical and horizontal components) measured by the T-28 during the first penetration were weak (Figure 7). Both components were negative throughout the entire penetration, and the magnitudes were only a few kV m^{-1}, near what is believed to be the uncertainty of the measurements. Also, there was no correlation between electric field measurements and updraft/downdraft structure or particle clusters. These measurements and earlier ones made by the P-3 indicate that electrification up to this point was relatively weak, at least in the vicinity of the penetrations.

3.2.3. T-28 penetration 2. The second penetration made by the T-28 began at 1840:30, 15 min after the initial radar echo. The aircraft entered the cloud on the northwest side, flew directly through the high Z_{DR} column and the high-reflectivity core, and exited through the southeastern edge of the cloud at 1842:00. At

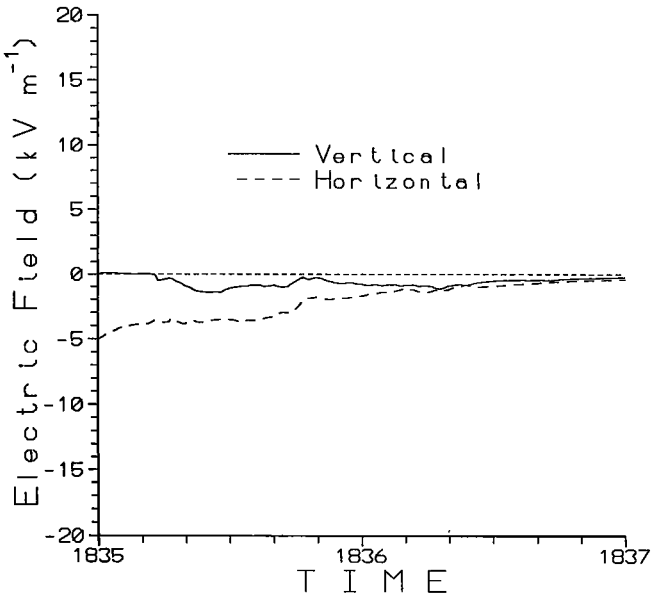

Figure 7. Ambient electric field (kV m^{-1}) derived from T-28 measurements during the first penetration. The solid line represents the vertical (z) component, and the dashed line represents the horizontal (y) component. See text for sign convention.

this time the storm was approximately 9 km long and 5.5 km wide, still arranged along a northwest to southeast axis. The high-reflectivity core (greater than 50 dBz) was located slightly northwest of the storm echo's center. Throughout much of the penetration the T-28 was in an area with reflectivities between 30 and 50 dBz, with greater reflectivities encountered earlier in the penetration.

Figure 8 shows a 5.25-km CAPPI with the T-28 flight track superimposed, and Figure 9a shows a cross section of reflectivity

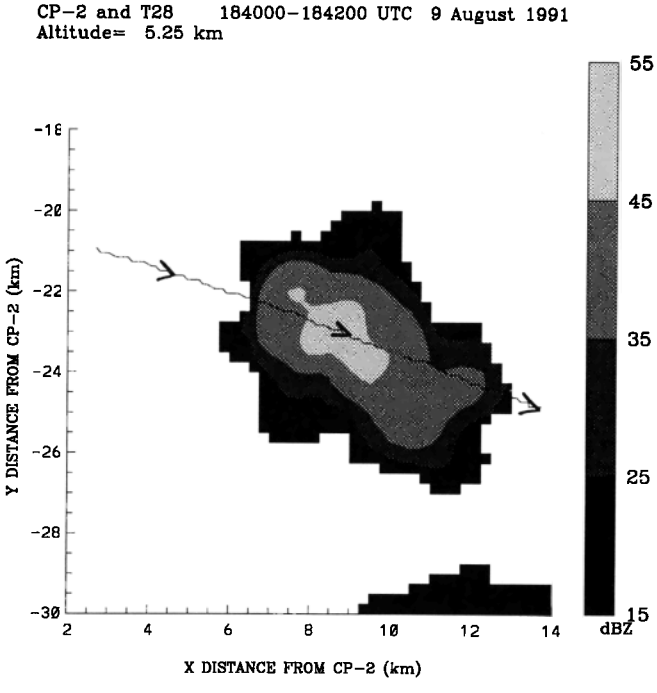

Figure 8. As in Figure 4, except for the second penetration, 1840:00-1842:00.

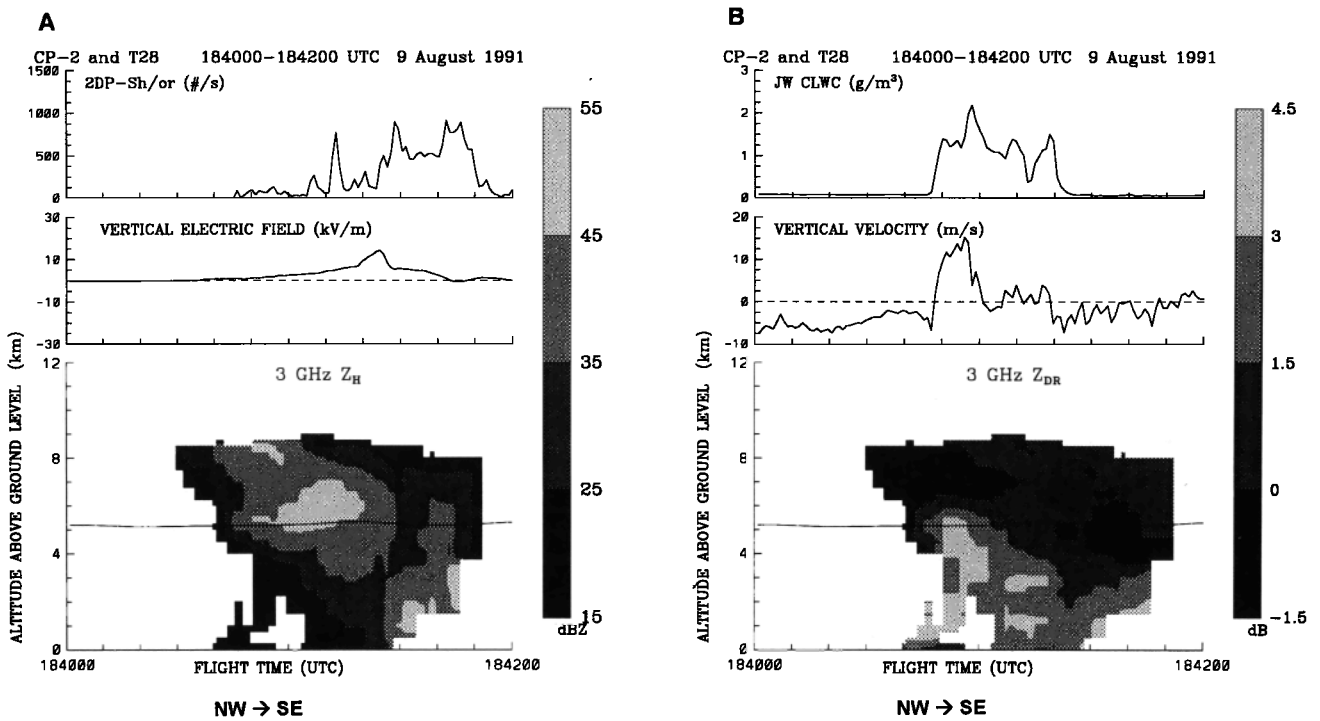

Figure 9. As in Figure 5, except for the second penetration.

along the flight path of the T-28, along with the vertical electric field and the 2D-P shadow/or count. Figure 9b shows the Z_{DR} cross section along the flight path along with the JW CLWC and the vertical wind. In the northwesternmost portion of the cloud (1840:48 to 1841:00) the T-28 encountered a narrow, moderate updraft with vertical speeds between 10 and 16 m s^{-1}. After exiting the updraft, the aircraft flew through a 2-km-wide "transition zone," where vertical velocities varied between −2 and +4 m s^{-1}. In this region, reflectivity values along the flight track were greatest (in excess of 50 dBz). In the downdraft region (1841:20 to 1841:48), vertical velocities were between −1 and −7 m s^{-1} and reflectivities were ~40 dBz. Shadow/or counts were much higher in the downdraft than they were in the updraft and transition zones.

Similar to the first T-28 penetration, the updraft had relatively high CLWC (JW readings between 1.5 and 2 g m^{-3}) and was collocated with a high Z_{DR} column. Throughout the updraft, Z_{DR} ranged from 1.5 to 3.5 dB. The 1.5-dB contour extended up to about 6.5 km (-12°C) in this region, again indicating the presence of supercooled raindrops. In the transition zone, which shared characteristics of both the updraft and the downdraft, the CLWC varied between 0.5 and 1.5 g m^{-3} and Z_{DR} ranged from 0.5 up to 2 dB. The presence of substantial liquid water, the absence of significant updraft, the moderately high reflectivity, the increasing precipitation particle concentration, and the particle images discussed below indicate that this region reflects the decay of a portion of the original updraft, probably due to precipitation loading. Note that the updraft has narrowed considerably in Figure 9b compared to Figure 5b, although the location remains the same with respect to the cloud structure. In the downdraft, which again was virtually devoid of any cloud liquid water, measured values for Z_{DR} were between −0.5 and 0.5 dB. This indicates that this portion of the storm was made up of graupel particles, which will be shown to be consistent with measurements made by the T-28 2D-P probe.

Images recorded by the 2D-P probe while the T-28 was in the updraft (1840:48 to 1841:00) are shown in Figure 10a. Concentration and size statistics are indicated in Table 1. The updraft was characterized by a number of streaker images. In the very beginning of the updraft (northwesternmost edge) a clustering of 11 particles ranging from 0.5 to 1 mm in diameter was detected in a region only 100 m across; this corresponds to a local concentration of nearly 70 m^{-3} of these larger particles. The foil impactor also detected this clustering, and the character of the impressions indicated that these particles were all liquid drops. About 2 s (~180 m) later, the 2D-P probe detected a very large liquid water drop with a diameter of 5.5 mm. This is a significant find, in that the T-28 was located in a region of very high Z_{DR} (~3.5 dB) with reflectivity of 43 dBz. This indicates that a relatively low concentration of large liquid-water drops can return high values of Z_{DR} together with moderate reflectivity. The foil impactor, despite sampling a similar volume, did not detect any drops of this size in the updraft. Seven other drops of diameter 1 to 2 mm were detected by both the 2D-P probe and the foil impactor throughout the remainder of the updraft. The total volume swept out by the 2D-P probe and foil impactor, each, in the updraft was approximately 2.4 m^3 (although 2D-P images were collected for only a fraction of this time).

Data from the 2D-P probe and foil impactor indicated the presence of both liquid water and ice particles in the transition zone. Figure 10b shows 2D-P images collected while the T-28 was in the transition portion of the storm. The presence of streaker images (fewer than in the updraft) indicates the continued presence of cloud liquid water; This agrees with measurements made by the JW probe. In the northwestern half of the transition zone (1841:00 to 1841:10; ~1 km) the 2D-P probe detected at least four particles with diameters greater than 2.5 mm in a sample volume of ~1.4 m^3. The two largest ones, ~7 mm diameter, appeared to be ice. Data from the foil impactor as well as the 2D-P images indicated that some of these particles were

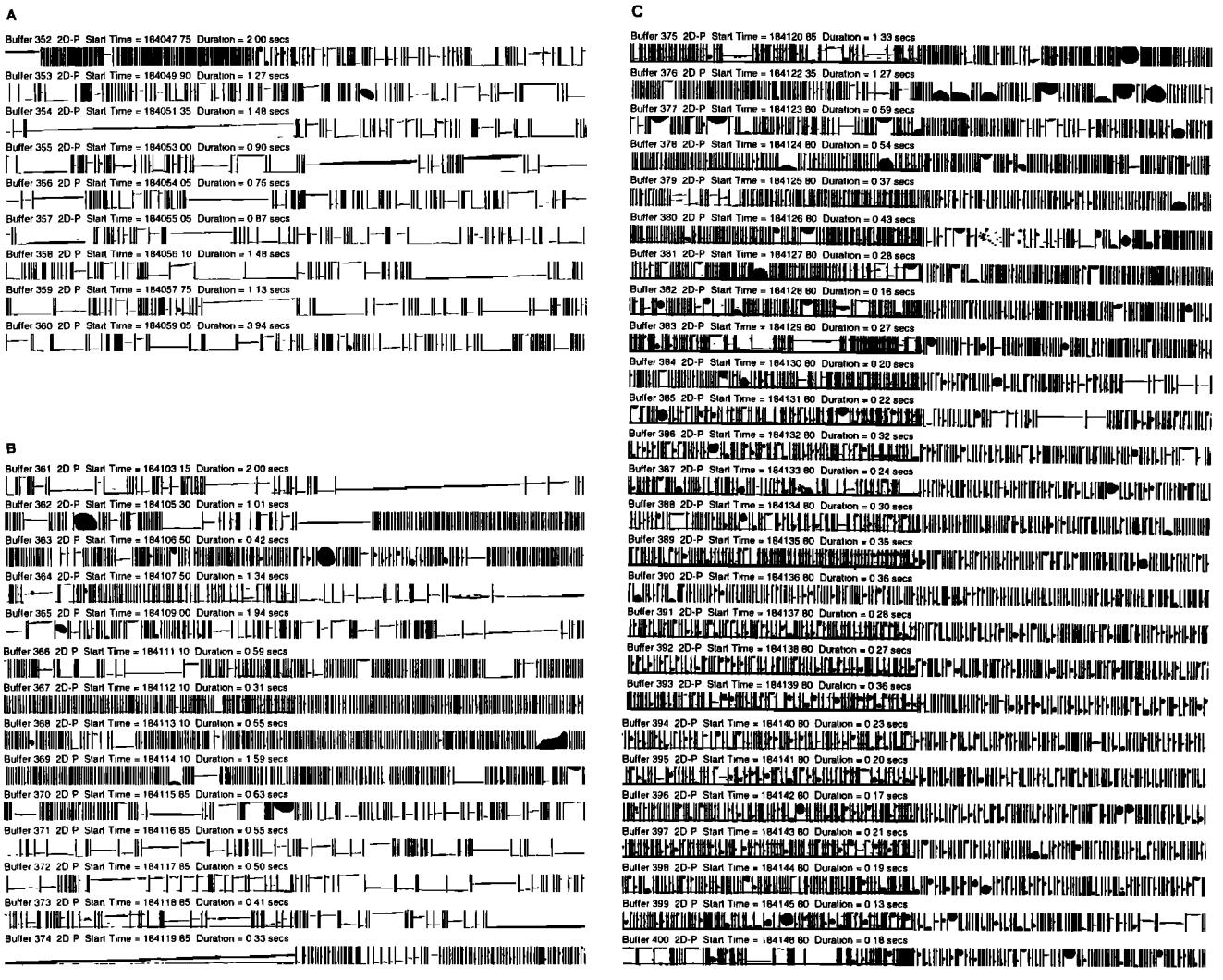

Figure 10. As in Figure. 6, except during the (a) updraft, (b) transition zone, and (c) downdraft in the second penetration. In this sample, all buffers are shown.

probably water drops, while some were probably graupel During the last 10 s (southeastern half) that the T-28 was in the transition zone, both devices detected a larger concentration of smaller particles, with only a few particles greater than 3 mm in diameter. Foil impactor data indicated that most, if not all, of the particles were ice.

Particle images from the first 0.5 km (1841:20 to 1841:25) of the downdraft (Figure 10c) indicated yet higher concentrations of small particles, and a relatively high number of particles greater than 3 mm in diameter. Those 2D-P images of sufficient size, and the foil impactor data, indicated that the particles detected in this region, as well as the rest of the downdraft, were ice As the T-28 flew farther through the downdraft, both devices indicated that rest of the downdraft was fairly homogeneous in particle sizes and concentrations, with somewhat fewer very small and very large particles.

The magnitudes of the electric field components measured during the second T-28 penetration (Figure 11) were significantly larger than those measured during the first penetration. The vertical component of the electric field was near zero as the T-28 entered the cloud from the northwest (1840.30). It increased almost linearly to about 7 kV m^{-1} at the far edge of the transition

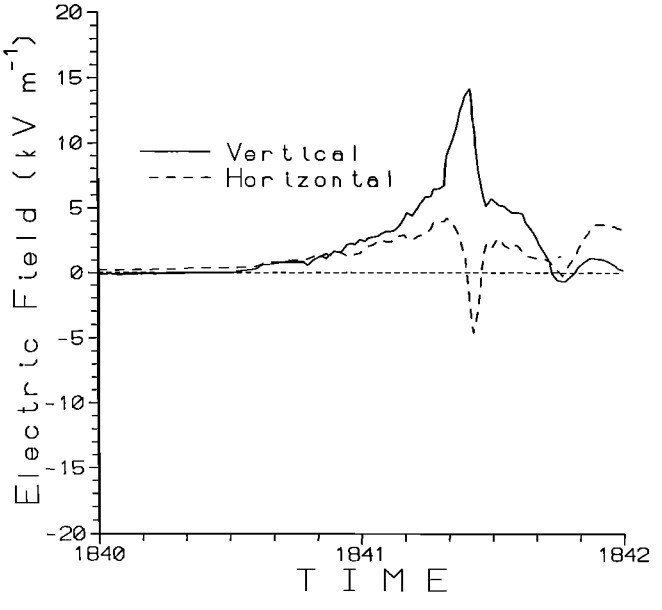

Figure 11. As in Figure 7, except for the second penetration.

zone (1841:20). The T-28 then experienced a relatively strong, positive, vertical component (up to 14 kV m^{-1}) over a span of 10 s (~0.9 km flight path) as it entered the downdraft. Figure 9 shows that the 2D-P probe particle detection rate (shadow/or count) increased dramatically in this region, while Figure 10c shows this to be a region with a mixture of small and large precipitation particles, predominantly ice. The vertical component of the electric field relaxed to zero as the T-28 flew on toward the southeastern edge of the cloud, through a region of higher concentrations of small graupel.

The horizontal component of the electric field (Figure 11) was smaller in magnitude, but its variation was similar in structure to the vertical component. The horizontal component increased linearly from zero (at 1840:30) to about 4.5 kV m^{-1} at 1841:20. This, coupled with the positive vertical component, indicated the presence of negative charge above and to the right (south) of the aircraft at this location. At the same location where the vertical component increased sharply, the horizontal component became negative (−5 kV m^{-1}). This is indicative of a localized region of negative charge slightly above and to the left (north) of the T-28 position. The horizontal component then recovered back to 3 kV m^{-1} and decreased to zero as the T-28 exited the cloud.

The electric field measurements throughout this penetration reflected some correlation with microphysical variables. In particular, the dominant peak in both resolved components of the electric field was encountered in the transition zone and northwest portion of the downdraft, in a region coincident with a relative maximum in the concentration of large graupel, as seen in Figure 10b.

The T-28 pilot reported lightning during this penetration near 1441:22, just before the peak in measured vertical and horizontal field components abruptly ended. Close examination of the individual T-28 field mill records indicates a small field change (£1 kV m^{-1}) at this time. Examination of data from several individual field mills in the Kennedy Space Center ground-based network shows indications of an intracloud discharge at this time but a more restrictive analysis [M. Murphy, personal communication, 1995) indicates the first resolvable intracloud lightning occurred at 1842:31, just after this penetration ended.

At 1845:00, while the T-28 was turning in preparation for a third penetration, the storm showed slow movement to the north, whereas it had been primarily stationary until this time (cf. Figure 3). The highest reflectivities at 5 km (over 60 dBz) were found in the center of the storm. This time corresponded to the highest reflectivity detected at the 5-km level during the entire life of the storm. At this level, the storm had a diameter of approximately 10 km. The high Z_{DR} column was located in the northwestern portion of the highest reflectivities at 5 km; the 1.5-dB contour extended up to about 6 km. The 1.5-dB contour was found at a height of about 4 km throughout the remainder of the high-reflectivity core, indicating graupel descending below the freezing level and melting.

3.2.4. P-3 penetration 2. The P-3 began making its second and final penetration at about 1845:00. It flew from the southeast to the northwest at an altitude of ~4.1 km (+3°C, ambient). The aircraft flew directly through the center of the storm and penetrated the high-reflectivity core (~60 dBz at this level).

The horizontal profile of vertical winds measured by the P-3 was consistent with that of the T-28 in its second penetration. In the center of the storm and to the southeast, downdrafts of about 2 to 4 m s^{-1} in magnitude were encountered. The northwestern side of the storm (corresponding to the Z_{DR} column) was made up of updrafts with relatively higher CLWC (King Probe readings to 3 g m^{-3}) and updrafts of 10 to 14 m s^{-1}.

The particle probes on the P-3 detected mainly graupel in the downdraft region, with a mixture of graupel and rain in the updraft region. Particle concentrations were generally lower than found by the T-28 4 min earlier and 1.1 km above, with generally similar peak sizes (cf. Table 1).

The electric field measured by the P-3 was consistent (in sign) with that measured by the T-28 during its second penetration. The P-3 encountered positive vertical electric fields throughout the penetration (the peak value of 4 kV m^{-1} occurred in the downdraft region), indicating net negative charge above the aircraft. The magnitude of the vertical component was relatively smaller than that measured by the T-28 1.1 km above. This can be interpreted as consistent with a region of negative charge above the T-28 altitude with the P-3 further removed from it and thus measuring a lower field magnitude. An induction ring instrument on the P-3 measured particle charges of both signs in the downdraft region, with an excess of negative particles over positive ones [*Brooks*, 1993]. No particle charge determinations could be made in the updraft region due to signal interference from water shedding from the induction ring.

3.2.5. T-28 penetration 3. The T-28 began making its third penetration from the east-southeast at 1847:30, some 22 min after the initial echo. The plane flew to the west-northwest, passing through the southern half of the highest reflectivities as shown in Figure 12. It passed about 2 km south of the high Z_{DR} column, which was then located in the northwesternmost portion of the storm. The T-28 was out of cloud by 1849:30.

A reflectivity cross section along the flight path of the T-28 (Figure 13a) reveals that the high-reflectivity core was located in the eastern half of the storm (beginning half of the penetration). The T-28 just penetrated the top of the region of highest reflectivities, which were between 55 and 60 dBz. The eastern portion of this core was located in a weak to moderate downdraft region

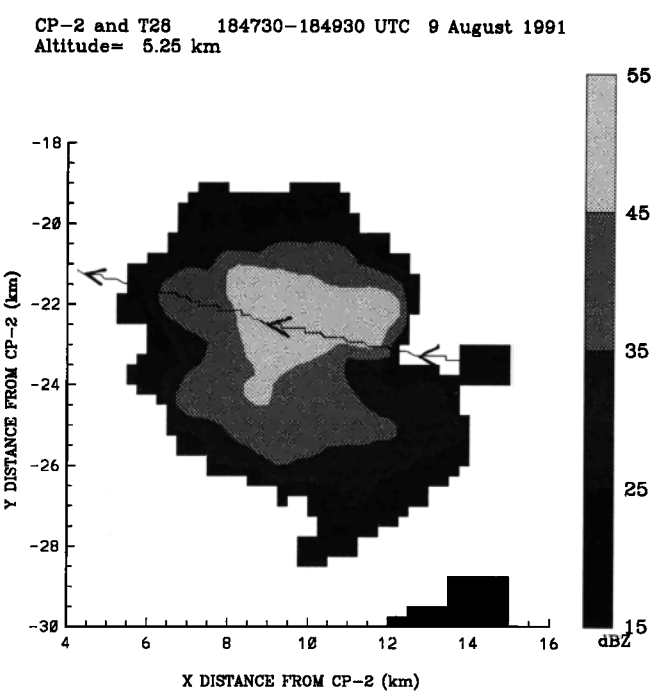

Figure 12. As in Figure 4, except for the third penetration, 1847:30-1849:30.

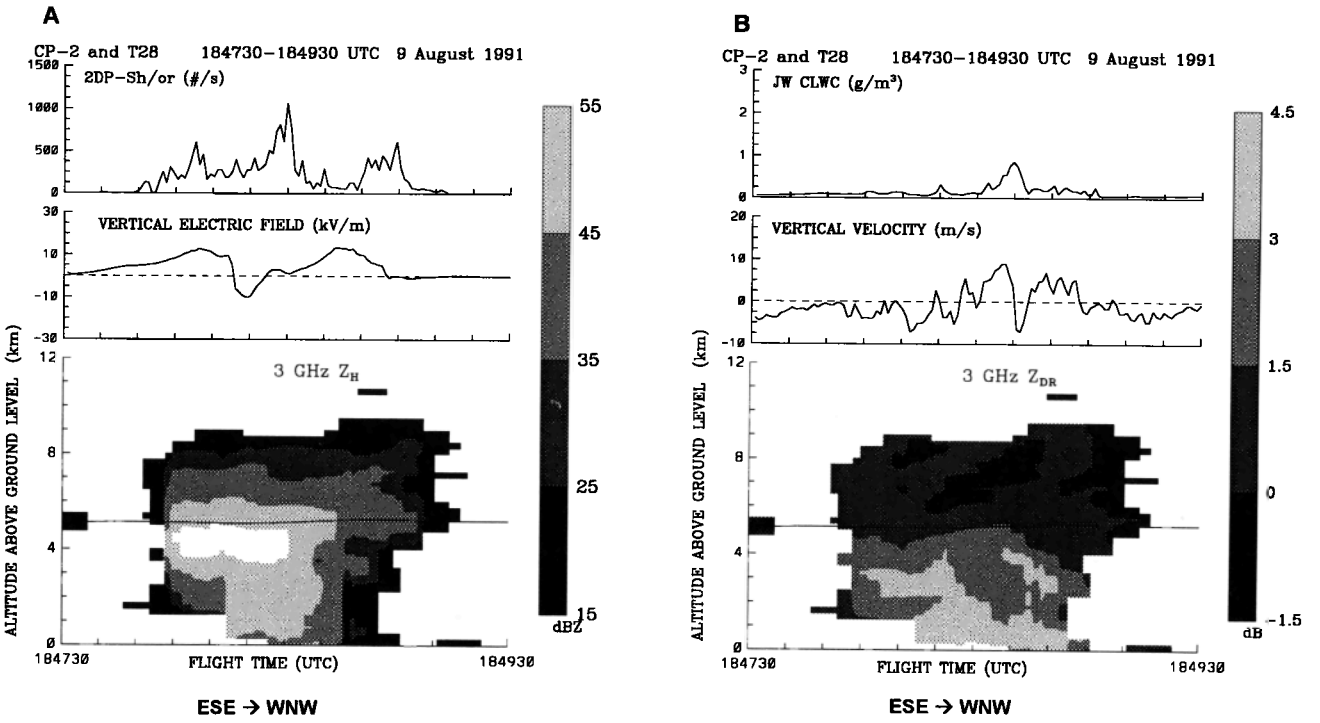

Figure 13. As in Figure 5, except for the third penetration.

(1847:50 to 1848:18) with a maximum negative vertical velocity of -7 m s^{-1} and moderate shadow/or counts. The western portion of the core was in the transition zone (1848:18 to 1848:30), where vertical winds between -5 and 5 m s^{-1} were encountered. In this region the shadow/or count peaked at over 1000 particles s^{-1}, corresponding to total 2D-P particle concentrations on the order of 6000 m^{-3}. The updraft (maximum ~10 m s^{-1}) was encountered on the northwesternmost edge and just outside of the reflectivity core. The shadow/or count was significantly lower in this region.

The Z_{DR} profile is shown in Figure 13b. Through much of the penetration, the 1.5-dB contour remained below the flight level of the aircraft. Yet, in the center of the updraft, the 1.5-dB contour did extend up to 5.25 km. This is also the region in which maximum CLWC was encountered (~0.7 g m^{-3}). North of the T-28 track, on the northwesternmost side of the reflectivity core, the 1.5-dB contour did extend above 6 km. The strongest updrafts were probably located in this region at this time.

Particle data revealed fewer differences between the various portions of the storm compared with earlier penetrations. In the southeastern portion of the downdraft (1847:51 to 1847:54) the 2D-P probe detected relatively low concentrations of small graupel particles, up to ~0.8 mm in diameter (Figure 14a and Table 1). For the next 0.5 km, the probe measured predominantly very small particles, but with maximum sizes steadily increasing with time to 2.2 mm at 1848:00. At this point, the T-28 entered an area of greater reflectivity (50 to 55 dBz). Throughout the rest of the downdraft region, data from both the 2D-P probe and foil impactor indicated higher concentrations of particles in all size categories, up to 6.6 mm in diameter. All of the particles detected in the downdraft appeared to be graupel.

There was no distinct boundary, at least in the particle types, between the downdraft region and the transition zone. The 2D-P images and statistics from the transition zone, 1848:18-1848:31 (Figure 14b and Table 1) revealed higher concentrations of larger graupel particles compared to the downdraft. The large number of "splatter" images evident in the PMS record should not be confused with streaker images. These splatter images are the result of mixed-phase precipitation particles hitting one of the probe tips and therefore there is no correlation between these images and high CLWC.

During the first 10 s (~0.9 km) of the updraft, 1848:32-1848:42, the T-28 flew through an area with a concentration of large particles similar to that in the transition zone (Table 1). This 1-km region corresponded to the highest reflectivities and Z_{DR} that were measured in the updraft on this penetration. Relatively fewer small particles (0.4 mm < d <1 mm) were detected in the updraft compared to the transition zone. Data from both the 2D-P probe (Figure 14c) and foil impactor were in agreement that the vast majority of the particles detected were ice (graupel), although some raindrops were present. Some of what appear to be streaker images are actually due to a stuck bit in the probe and do not represent real images (a stuck bit is generally represented by a perfectly "straight" image, that is, only one pixel, 0.2 mm wide). During a narrow downdraft that followed, and the remainder of the updraft (ending at 1849:00), both devices revealed a broad size distribution with higher concentrations than in the main updraft portion of the penetration. Many of the particles detected in this region appeared to be liquid, and splatter images indicative of mixed-phase particles are also evident.

The peak magnitude of the vertical electric field component during the third penetration was not much different than that during the second penetration, but the horizontal component was much larger than that measured during the second penetration (Figure 15). The vertical component of the electric field was positive through the first 40 s (~3.6 km) of the penetration. From this point, the field decreased dramatically over a 10-s period (~ 0.9 km) and went through a minimum of approximately

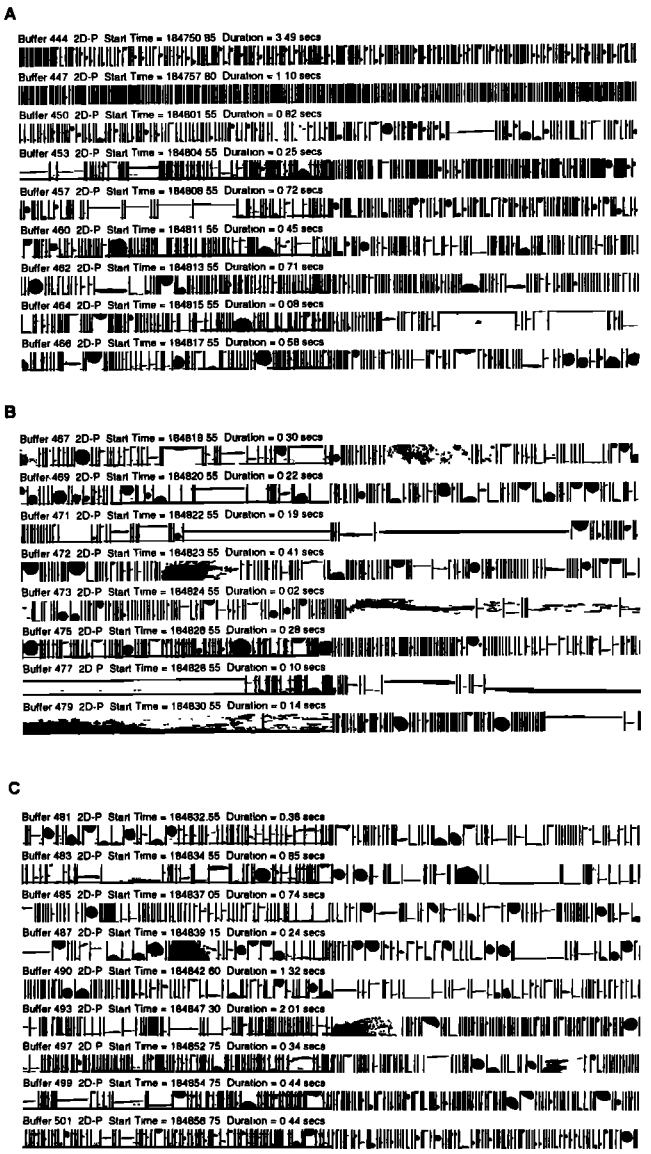

Figure 14. As in Figure 6, except for during the (a) downdraft, (b) transition zone, and (c) updraft in the third penetration.

−10 kV m^{-1} at the edge of the downdraft region at 1848:18. The vertical component of the electric field then recovered to 13 kV m^{-1} and then decreased to zero as the T-28 crossed the fringe of the updraft region and approached the northwestern edge of the cloud.

The measured horizontal component of the electric field was opposite in sign from that measured during the second penetration. This is consistent with the second penetration, since the T-28 was flying in the opposite direction. The horizontal component decreased from zero at the southeastern edge of the cloud to a minimum of −20 kV m^{-1} about 40 s into the penetration, coincident with the maximum in the vertical component in the downdraft region. The T-28 then passed through an area at 1848:30 where the horizontal component was a relative maximum (0 kV m^{-1}). This location corresponded to the boundary between the transition region and the updraft, and a shift in sign of the vertical component, indicating a localized region of relatively high positive charge density above and to the left (south), or negative charge below and to the right (north), of the position of the aircraft at this time The horizontal component recovered to about −7 kV m^{-1} and then decreased as the T-28 crossed the fringe of the updraft and approached the northwestern edge of the cloud.

Much more variation in the electric field was measured by the T-28 during this penetration than in the two earlier penetrations. When the vertical component reached its most negative value (1848:18), the T-28 was in the most significant downdraft measured during that penetration. Yet, the particle phases, sizes, and concentrations during this time were similar to those sampled before and after this downdraft was encountered. One interpretation of these observations is that the T-28 was close in altitude to the center of a negative charge layer, and that the center altitude of this region was below the aircraft in the downdraft and above it elsewhere.

4. Summary of Observations

The early electrical evolution of this storm was strongly coupled with the evolution of the storm's microphysics For this reason, we summarize here the evolution of the storm as a whole and do not break it into electrical and nonelectrical components.

The P-3 penetrated the storm near the time and level of the first radar echo. It detected a few small precipitation-size ice particles at the −10°C level, but no significant electric fields. Eight minutes later, the T-28 penetrated at the −3°C level. It detected significant concentrations of precipitation-size particles in the downdraft (mostly ice) and only a few precipitation-size particles (mostly liquid) in the updraft. Electrification up to this point had remained relatively weak.

Five minutes after the T-28's first penetration, it again flew through the storm at the −3°C level It encountered significant concentrations of precipitation-size particles Moderate updrafts were encountered, which contained the lowest concentration of precipitation-size particles. The observations are consistent with liquid particles in the updraft growing by collision/coalescence and then being carried upward, where they would freeze at temperatures between −5° and −10°C. This interpretation is supported by the Z_{DR} profile Also, high concentrations of ice particles (graupel) were detected in the downdraft. These particles

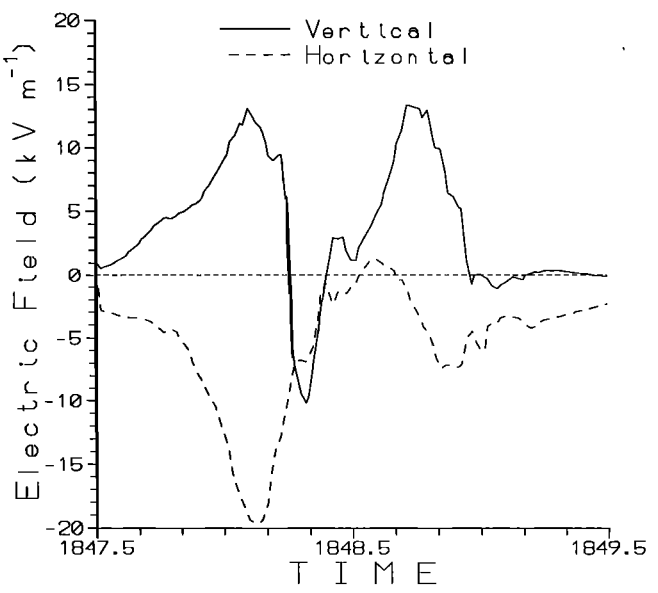

Figure 15. As in Figure 7, except for the third penetration.

did not melt until they were well below the level of the aircraft, as was evident from subsequent P-3 observations about 1 km lower in altitude.

The electrical character of the storm had changed significantly during the 5-min interval between the times of the first two penetrations. Such rapid development of electrification has been noted in studies of other CaPE storms [e.g., *Willis et al.*, 1994, *Ramachandran et al.*, 1996] and in similar studies of thunderstorms elsewhere [e g., *Dye et al.*, 1986, 1988]. During the second penetration, vertical electric fields of the order of several kV m^{-1} were measured at the level of the T-28 From these measurements and ones made during earlier penetrations, it is obvious that there was a definite lag between the initiation of precipitation-size particles and the rapid buildup of the electric field. This delay is not surprising; it has been documented several times [e.g., *Reynolds and Brook*, 1956; *Dye et al.*, 1986]. In both of these earlier studies the delay was of the order of 8 to 10 min, while we found a delay of 11 to 17 min. Whether this difference is significant is open to debate, but one possible explanation is that in the earlier studies, precipitation was initiated through ice processes. In our case, precipitation was initiated at higher temperatures through collision/coalescence. If ice plays a significant role in the electrification of thunderstorms (as suggested by precipitation-based electrification hypotheses), we would expect a longer delay in coalescence-dominated clouds.

An interesting feature found in the electric field profile during the second T-28 penetration is that the maximum seems to occur between the transition and downdraft regions and is nearly coincident with the region of highest reflectivity. This too has been documented in earlier studies [*Dye et al.*, 1986, 1988; *Willis et al.*, 1994]. This finding supports the idea of a precipitation-based charging mechanism active in this cloud. It is in the transition zone where one would expect to find the greatest number of different particle types (graupel, snow, cloud ice, etc.) Also, in this region, CLWC would be large enough to allow riming of the graupel particles (a very important requirement for non-inductive charging to take place). Without measurements of actual particle charge at this and other levels in this storm, it is impossible to determine to what extent charge separation may have been taking place in the transition zone However, the idea of charging in this region is consistent with our measurements

The P-3 made its second penetration about 3 min after the T-28 exited the cloud from its second pass The P-3 flew significantly lower than in the earlier penetration (4 1 km, ~3°C) The electric field profile measured by the P-3 was considerably smaller in magnitude but consistent in sign with that measured by the T-28 during its second penetration These measurements are consistent with a large region of negative charge located above the flight level of the T-28. The greater distance between the P-3 and the charge region, and possible rearrangement of the charge distribution due to the lightning discharge, could account for the weaker fields observed by the P-3. It is also possible that some of the reduction in the strength of the electric field (with decreasing altitude) was due to a region of weak positive charge located between the two flight levels (4 1 and 5.25 km, +3° and −3°C); however, it is impossible to tell if this is the case from the data.

The third penetration made by the T-28 began about 2 min after the P-3's second penetration Again, the T-28 flew at 5 25 km. This penetration was offset from the most active convection within the storm (south of the high Z_{DR} column). The measured horizontal component of the electric field was also relatively large, indicating that the aircraft was not on the main electrical axis either. With the development of lightning and of a second convective region (or the movement and reinvigoration of the original one) the distribution of charge within the storm has become more complex by this time.

5. Discussion

The evolution of this storm can be divided into two main parts. First is the early evolution prior to any indications of electrification, including the time from first echo through the next 12 to 15 min. The first penetrations of both the P-3 and the T-28 were made during this time. The second part of this storm's evolution consists of the following 10 to 15 min of its lifetime. During this period, the T-28 made two penetrations, the P-3 made its last penetration, and electrical activity became evident. After this second "evolution period" the storm began to enter its decaying stage (microphysically and dynamically). We did not analyze this final time period in detail, above.

5.1. First Stage

The first 12 to 15 min in the evolution of this storm was characterized by broad updrafts reaching 14 m s^{-1} and containing CLWC ranging up to at least 4 g m^{-3} initially (as measured by the P-3 King Probe; the T-28 JW readings later in this period are probably an underestimate of the true CLWC) Concentrations of medium to small raindrops ($0.4 < d \leq 1.5$ mm) ranged up to almost 1000 m^{-3}. Downdrafts during this period were broad and ranged to −10 m s^{-1}. The downdraft region was devoid of cloud liquid water. The majority of the particles in this region were ice ($d \leq 2$ mm) yet a few raindrops were detected in the transition zone near the edge of the downdraft within a kilometer of the updraft region.

Our analysis is consistent with a coalescence-dominated convective storm in which raindrops form and grow in an updraft region that is rich in cloud liquid water These raindrops are carried via the updrafts to levels above the 0°C isotherm The Z_{DR} column (collocated with the updraft and indicative of larger raindrops) extended to about 6 km throughout this portion of the storm's evolution. This height corresponds to approximately −10°C. At this level, even the smaller raindrops would begin to freeze and the newly formed graupel, with diameters of 3 mm or less, would continue to grow through accretion of cloud and rain water.

It is also probable that cloud ice would be formed through the Hallet-Mossop process [*Hallet and Mossop*, 1974] near this level in the updraft, given the temperature, high CLWC, broad cloud droplet size distribution characteristic of warm-base clouds, and the existence of graupel These crystals would grow fairly quickly through deposition, since the environment should be highly supersaturated with respect to ice. Aggregation of these ice crystals should also lead to the production of snow that could then rime and represent another source of graupel.

At higher levels, some of the recently formed graupel began to fall out of the updraft, into the downdraft. Loading of the updraft may in fact have helped to produce the upper-level downdraft at about the same time rain began to freeze. As this occurred, the leading portion of the updraft region propagated northwestward at lower levels. Much of the graupel in the downdraft region was less than 2 mm in diameter. Particle concentrations in this downdraft region were much higher than in the updraft, with the

highest concentrations (nearly 1000 m^{-3}) found in that portion of the downdraft nearest the updraft. This, coupled with the low concentrations in the updraft, explains the pattern of moderate reflectivity throughout much of the downdraft with the highest reflectivities in the transition zone, between the updraft and downdraft, on the edge of the Z_{DR} column. The weakest reflectivities were collocated with the updraft and the Z_{DR} column.

Electrification, throughout this early stage in the storm's evolution, was extremely weak. This is to be expected if charge transfer and separation were based on some type of precipitation mechanism involving ice-phase particles. Throughout this period, concentrations of ice particles remained relatively low. Also, it was not until the end of this period that significant reflectivities, implying higher concentrations of graupel, were found to exist at temperatures of −20°C. Significant charge transfer via a noninductive mechanism requires reasonably high concentrations of graupel and snow and/or cloud ice in the −20°C region [e.g., *Takahashi*, 1978a; *Saunders*, 1993]. If the concentrations are not high enough, there will be too few collisions between these particles to lead to strong electrification. Although some charge transfer may have taken place at and around −10°C with graupel and cloud ice (formed through the Hallet-Mossop mechanism), it is not clear from the observations what effect this may have had on the large-scale electrification of this storm. This question will be addressed further in the companion modeling paper.

5.2. Second Stage

The next portion of the storm's evolution was characterized by a narrower updraft and a more broad, diffuse, downdraft. The regions were separated by a 1- to 2-km-wide transition zone which had weak to moderate updrafts and downdrafts The updraft was rich in cloud liquid water (peak JW readings of 2 g m^{-3}) but was relatively free of precipitation-size particles (hundreds m^{-3}) The downdraft was characterized by very little cloud liquid water and high concentrations (many thousand m^{-3}) of graupel. The transition zone shared characteristics of both the updraft and downdraft. In this region, CLWC was moderate (~1 g m^{-3}) and precipitation particle concentrations were also moderate (many hundred to a few thousand m^{-3}). Some particles detected in this region were ice, while others were mixed phase or liquid

Measurements made during this portion of the storm's lifetime seem to present a consistent view of how the storm evolved microphysically from being dominated by liquid coalescence processes to being dominated by ice-phase processes. Raindrops would form and grow in the updraft region and be carried to higher regions in the storm, where they would freeze forming graupel. Also, during this stage, significant amounts of cloud ice were most likely being produced through heterogeneous freezing of cloud droplets at higher levels in the storm (although we obtained no in situ observations at these levels to verify this conjecture). Ice crystals produced through this and other mechanisms would grow by diffusion and aggregate to form snow, which could then serve as graupel embryos, although raindrop freezing is probably the primary graupel production mechanism We would expect the graupel to continue to grow by accretion in the updraft and transition zone until these particles became part of a downdraft. Microphysically, this is the same process as described for the early portion of the storm evolution. The main difference is that, in the mature phase, the process takes place over a larger depth and therefore more and larger particles are produced.

During this portion of the storm's evolution, it went through a rapid increase in electrification, as evidenced by the observed increase in electric field strength at the aircraft penetration levels. This is consistent with a precipitation-based mechanism being responsible for the electrification As graupel and cloud ice both began to appear in significant concentrations at low temperatures (−20°C), appreciable charge transfer and separation would be expected to occur according to the noninductive charge-transfer processes studied in the laboratory [*Takahashi*, 1978a; *Saunders et al.*, 1991]. When particles (graupel/cloud ice and/or graupel/snow) collide in regions of this temperature and in the presence of cloud liquid water, the graupel acquires negative charge and cloud ice and/or snow acquires positive charge. If these interactions were taking place in the transition region (where all the necessary components were present), we would expect graupel to be charged negatively and snow and cloud ice to be charged positively.

As the graupel particles fall out, the negative charges are carried downward, away from the region of production This leads to large-scale charge separation. We envision this process continuing, leading to a region of negative charge above the aircraft penetration levels, and positive charge at even higher altitudes. This process continues and electric fields build up to the point, near 1842:00, when lightning was detected. Further increases in electric field strength, as measured by the T-28, most likely are the result of two phenomena First, as charge continues to be separated well above the 0°C level, electric fields will continue to increase. Second, since the negative charge is associated with graupel descending in the downdraft, we might expect the main negative charge region to descend with time. Although the magnitude of the charge in this region may not be increasing, the electric fields at the level of the T-28 would continue to increase as the descending center of mass of the charged graupel approached the aircraft altitude from above. As the center of this charge layer passes through the aircraft penetration levels in downdraft regions, the sign of the vertical field component reverses

Concluding Remarks

Although we cannot be sure of all of the elements envisioned in this discussion of the evolution of the August 9 storm, we have presented a "story" that is consistent with the measurements. We also quantitatively described how the storm evolved both microphysically and electrically. In a companion paper, we attempt to capture this evolution in a numerical simulation using the two-dimensional Storm Electrification Model (2-D SEM) and quantitatively compare the simulated to the observed storm.

Acknowledgments. We wish to thank V. N Bringi and J. Turk for radar analysis software used in generating several of the figures; K. Hartman for generating the particle images; D. Priegnitz for help in creating some of the radar figures; and C. P. R. Saunders, I. Brooks, and R Black for providing the NOAA P-3 data. This research was supported by the National Science Foundation under grants ATM-9104474, ATM-9401117, ATM-9022846, ATM-9509810, and ATM-9200698.

References

Aufdermaur, A. N., and D. A. Johnson, Charge separation due to riming in an electric field, *Q. J. R. Meteorol. Soc*, *98*, 369-382, 1972.

Black, R. A., and J. Hallet, Observations of the distribution of ice in hurricanes, *J. Atmos. Sci.*, *43*, 802-822, 1986.

Bringi, V. N., and A. Hendry, Technology of polarization diversity radars for meteorology, in *Radar Meteorology*, edited by D. Atlas, pp. 153-190, Am. Meteorol. Soc., Boston, Mass., 1990.

Bringi, V. N., A. Detwiler, V. Chandrasekar, P. L. Smith, L. Liu, I. J. Caylor, and D. Musil, Multiparameter radar and aircraft study of the transition from early to mature storm during CaPE: The case of 9 August 1991, in *26th International Conference on Radar Meteorology, Norman, OK*, pp. 318-320, Am. Meteorol. Soc., Boston, Mass., 1993.

Brooks, I. M., Laboratory studies of thunderstorm charging processes, Ph.D. thesis, 164 pp., Univ. of Manchester, Manchester, England, 1993.

Brooks, I. M., and C. P. R. Saunders, An experimental investigation of the inductive mechanism of thunderstorm charging, *J. Geophys. Res., 99*, 10,627-10,632, 1994.

Church, C. R., The electrification of hail, Ph.D. thesis, pp. 55-57, Univ. of Durham, Durham, England, 1966.

Dye, J. E., J. J. Jones, W. P. Winn, T. A. Cerni, B Gardiner, D. Lamb, R. L. Pitter, J. Hallet, and C. P. R. Saunders, Early electrification and precipitation development in a small, isolated Montana cumulonimbus, *J. Geophys. Res., 91*, 1231-1247, 1986.

Dye, J. E., J. J. Jones, A. J. Weinheimer, and W. P. Winn, Observations within two regions of charge during initial thunderstorm electrification, *Q. J. R. Meteorol. Soc., 114*, 1271-1290, 1988.

Elster, J., and H. Geitel, Zur Influenztheorie der Niederschlagselektrizität, *Phys. Z., 14*, 1287, 1913.

Foote, B., Scientific overview and operations plan for CaPE, 145 pp., Natl. Cent. for Atmos. Res., Boulder, Colo., 1991.

Giori, K. L. and J.E. Nanevicz, Comparison of the electrical charging and discharging environments of multiple aircraft-borne electric field measurement systems, in *Proceedings, 15th International Aerospace and Ground Conference on Lightning and Static Electricity*, 27-1–27-10. U.S. Dept. of Transportation, Atlantic City, N.J., 1992.

Goodman, S. J., D. E. Buechler, P. D. Wright, W D. Rust, and K. Nielsen, Polarization radar and electrical observations of microburst producing storms during COHMEX, in *Proceedings, 24th Conference on Radar Meteorology*, pp. 109-112, Am. Meteorol. Soc., Boston, Mass., 1989.

Grenet, G., Essai d'explication de la charge electrique des nuages d'orages, *Extrait Ann. Geophys., 3*, 306, 1947.

Hallet, J., and S. C. Mossop, Production of secondary ice particles during the riming process, *Nature, 249*, 26-28, 1974.

Herzegh, P. H., and A. R. Jameson, Observing precipitation through dual-polarization radar measurements, *Bull. Am. Meteorol. Soc., 73*, 1365-1374, 1992.

Illingworth, A. J., The formation of rain in convective clouds, *Nature, 336*, 754-756, 1988.

Jacobson, E. A., and E. P. Krider, Electrostatic field changes produced by Florida lightning, *J. Atmos. Sci., 33*, 103-117, 1976.

Jayaratne, E. R., C. P. R. Saunders, and J. Hallett, Laboratory studies of the charging of soft-hail during ice crystal interactions, *Q. J. R Meteorol. Soc., 109*, 609-630, 1983.

Jones, J. J., W. P. Winn, and F. Han, Electric field measurements with an airplane: Problems caused by emitted charge, *J. Geophys. Res., 98*, 5235-5244, 1993.

King, W. D., J. E. Dye, J. W. Strapp, D. Baumgardner, and D. Huffman, Icing wind tunnel tests on the CSIRO liquid water probe, *J. Atmos. Ocean Technol., 2*, 340-352, 1985.

Knight, C. A., N. C. Knight, W. W. Grotewold, and T. W. Cannon, Interpretation of foil impressions of water and ice particles, *J. Appl. Meteorol., 16*, 997-1002, 1977.

Kopp, F. J., Deduction of vertical motion in the atmosphere from aircraft measurements, *J. Atmos. Ocean Technol., 2*, 684-688, 1985.

Krehbiel, P. R., An analysis of the electric field charge produced by lightning. Ph.D. thesis, 400 pp , Inst. of Sci. and Technol., Univ. of Manchester, Manchester, England, 1981.

Krehbiel, P. R., Electrical structure of thunderstorms, in *The Earth's Electrical Environment*, pp. 90-113, Natl. Acad. Press, Washington, D.C., 1986.

Krider, E. P., Electric field changes and cloud electrical structure, *J. Geophys. Res., 94*, 13,145-13,149, 1989.

Latham, J., and B. J. Mason, Electric charging of hail pellets in a polarizing electric field, *Proc. R. Soc. London, A, 266*, 387-401, 1962.

Lhermitte, R. M., and E. R. Williams, Thunderstorm electrification: A case study, *J. Geophys. Res., 90*, 6071-6078, 1985.

Lucas, C., E. J. Zipser, and M. A. LeMone, Convective available potential energy in the environment of oceanic and continental clouds: correction and comments, *J. Atmos. Sci., 51*, 3829-3820, 1994.

Maier, L. M., and E. P. Krider, The charges that are deposited by cloud-to-ground lightning in Florida, *J. Geophys. Res., 91*, 13,275-13,289, 1986

Miller, A. H., P. B. MacCready Jr., and D. M. Takeuchi, Cloud physics observations in South Dakota cumulus clouds, *Rep. MR167 FR-626*, 59 pp., prepared for Inst. of Atmos Sci by Meteorol. Res. Inc., Altadena, Calif., 1967.

Murphy, M. J., E. P. Krider, and M W. Maier, Lightning charge analyses during small CaPE storms, *J. Geophys. Res.*, in press, 1996

Ramachandran, R., A.G. Detwiler, J.H. Helsdon Jr., P.L. Smith, and V.N. Bringi, Precipitation development and electrification in Flordia thunderstorm cells during Convection and Precipitation/Electrification (CaPE) experi ment, *J. Geophys. Res., 101*, 1599-1619, 1996.

Reynolds, S. E., and M. Brook, Correlation of the initial electric field and the radar echo in thunderstorms, *J. Meteorol., 13*, 376-380, 1956.

Reynolds, S. E., M. Brook, and M. F. Gourley, Thunderstorm charge separation, *J. Meteorol., 14*, 426-437, 1957.

Saunders, C. P. R., A review of thunderstorm electrification processes, *J. Appl. Meteorol., 32*, 642-655, 1993.

Saunders, C. P. R., Thunderstorm electrification, in *Handbook of Atmospheric Electrodynamics*, vol. I, edited by H. Volland, pp. 61-92, CRC Press, Boca Raton, Fla., 1995.

Saunders, C. P. R., W. D. Keith, and R P Mitzeva, The effect of liquid water on thunderstorm charging, *J. Geophys. Res., 96*, 11,007-11,017, 1991.

Takahashi, T., Riming electrification as a charge generation mechanism in thunderstorms, *J. Atmos. Sci., 35*, 1536-1548, 1978a

Takahashi, T., Electrical properties of oceanic tropical clouds at Ponape, Micronesia, *Mon. Weather Rev., 106*, 1598-1612, 1978b.

Takahashi, T., Near absence of lightning in torrential rainfall producing Micronesian thunderstorms, *Geophys. Res. Lett., 17*, 2381-2384, 1990.

Vonnegut, B., Possible mechanism for the formation of thunderstorm electricity, *Bull. Am. Meteorol. Soc., 34*, 378-381, 1953.

Willis, P. T., J. Hallet, R. A. Black, and W. Hendricks, An aircraft study of rapid precipitation development and electrification in a growing convective cloud, *Atmos. Res , 33*, 1-24, 1994.

Winn, W. P., Aircraft measurements of electric field Self-calibration, J. Geophys. Res., 98, 7351-7365, 1993.

A.G. Detwiler, J.H. Helsdon, and P.L. Smith, Institute of Atmospheric Sciences, South Dakota School of Mines and Technology, 501 E. St. Joseph Street, Rapid City, S.D. 57701-3995. (e-mail: jhelsdon@lightning.ias.sdsmt.edu).

J.R. French, Department of Atmospheric Sciences, University of Wyoming, Laramie, WY 82070.

(Received April 26, 1995; revised November 27, 1995; accepted January 23, 1996.)